Research Square

Preprints are preliminary reports that have not undergone peer review.
They should not be considered conclusive, used to inform clinical practice,
or referenced by the media as validated information.

The study of O-GalNAcylation repair on MUC2 and E-cadherin of intestinal epithelial cells damaged by lipopolysaccharides

Aohang Yu
Northwest A&F University
Chihao Wang
Northwest A&F University
Chaojie Chen
Northwest A&F University
Yumeng Wang
Northwest A&F University
Chenchen Wu
wucen958888@163.com
Northwest A&F University

Research Article

Keywords: O-GalNAc, E-cadherin, MUC2, O-glycosylation, Lipopolysaccharide

Posted Date: July 15th, 2026

DOI: https://doi.org/10.21203/rs.3.rs-10049429/v1

License: This work is licensed under a Creative Commons Attribution 4.0 International License.
Read Full License

Additional Declarations: No competing interests reported.

The study of O-GalNAcylation repair on MUC2 and E-cadherin of intestinal epithelial cells damaged by lipopolysaccharides

Aohang Yu, Chihao Wang, Chaojie Chen, Yumeng Wang, Chenchen Wu[#]
College of Animal Veterinary Medicine, Northwest A&F University, Yangling, Shaanxi 712100, China
[#] Correspondence: Chenchen Wu, Phone number:+8618292176859, E-mail:wucen95888@163.com

Abstract

The intestine harbours the most extensive reservoir of bacteria and endotoxins in the body, with its mucosal immune system acting as the primary defensive barrier. Mucin-2 (MUC2) is a major component of the mucosal layer. A previous study reported that increased MUC2 expression could attach and repair the Adherens junction of intestinal epithelial cells and reduce lipopolysaccharide (LPS) translocation. However, the mechanism by which MUC2 repairs the adherens junction structure remains unclear.

In this study, we found that MUC2 specifically interacts with E-cadherin. LPS mainly alters the O-GalNAcylation of MUC2 and damages the structure of the endoplasmic reticulum in intestinal epithelial cells, resulting in a decrease and loss of O-glycan abundance and long-chain O-glycans in MUC2, all of them were mainly HexNAc O-glycosylation pattern. In contrast, O-glycosylation of E-cadherin shows no change. GalNT3 overexpression, along with the new addition of long-chain O-glycans and upregulation of Core-3 O-glycan chain abundant on MUC2, that the O-glycan scaffold structure of MUC2 was restored even under continuous LPS exposure. The trends for the E-cadherin and MUC2 proteins content are consistent in LPS and LPS+oe-GalNT3 group. MUC2 restores the structure of E-cadherin under conditions of rised Ca^{2+} content, that is mainly due to the O-glycosylated proteins were mainly involved in Calcium-binding EGF domain, and Adherens junction pathway were enrichmented by KEGG, Meanwhile, Go description showed that GALNT3 overexpression upregulated O-GalNAc glycosylation protein (PLXNB1, ERP44, CD320, CD44, AGRN, NUCB1 and CANX), maintained intracellular Ca^{2+} homeostasis and enhanced the mucosal barrier integrity in intestinal. The dual actions

of MUC2 and E-cadherin together reduced the cellular injury caused by LPS translocation and provided a new research direction for the repair of intestinal mucosal immune barrier function.

Keywords: O-GalNAc/E-cadherin/MUC2/O-glycosylation/Lipopolysaccharide

1.Introduction

Lipopolysaccharide (LPS) is the main component of endotoxins in the cell wall of Gram-negative bacteria. It is released upon bacterial cell death and lysis, and is also continuously released during bacterial growth and reproduction. The mucus layer acts as the first line of defence against the entry of bacteria and their endotoxins into the body through the digestive and respiratory tracts (Jiaoling Wu *et al.* 2024; Jiaoling Wu *et al.* 2020; Paone *et al.* 2020; Nystrom *et al.* 2020). Mucin-2 (MUC2) is the main component of the mucus layer and is secreted by goblet cells. MUC2 is heavily O-glycosylated on its protein sequence rich in proline, threonine, and serine; O-glycosylation mainly occurs in the rough endoplasmic reticulum and Golgi complex (Mengyuan *et al.* 2024; Laubli *et al.* 2019; Jayaprakash *et al.* 2017). In a previous study, we found that MUC2 increased its expression levels and spatial distribution, contributing to the restoration of tight junction structures in cells with larger intercellular gaps after LPS treatment. Further, strengthening of the barrier prevents endotoxin translocation by repairing the tight junction structure of epithelial cells (Dujian *et al.* 2024). Beneath the mucus layer lie the tight junctions and adherens junctions of epithelial cells **(**McEver *et al.* 2002**)**. Adherens junctions are cell–cell adhesion complexes that transmit mechanical signals across the epithelium to coordinate development and tissue homeostasis dynamics **(**Mingming Zhang *et al.* 2022**)**. However, we are still unclear about how MUC2 repairs tight and adherens junctions structures under the LPS? Therefore, in this study, we further explore the mechanism by which O-glycosylated MUC2 and tight junction structures interact and strengthen the defence barrier of the intestinal mucus layer in Caco-2/HT29 cells. Our results elucidate the mechanisms by which healthy mucins attenuate bacterial and toxin pathogenicity and suggest therapeutic candidates for treating bacterial infections without disrupting the microbiota.

2. Materials and methods

2.1 Caco-2/HT29 co-culture cells

Caco-2 (BNCC Bio-350769, China) and HT-29 (BNCC Bio- 350769, China) cells were seeded at a density of 1×10^5 cells/cm^2. The cells were grown in tissue culture flasks at 37°C with 5% CO_2 and 90% relative humidity. All cell lines were maintained in DMEM-H medium (containing glutamine and sodium pyruvate) supplemented with 10% fetal bovine serum and 1% penicillin-streptomycin. The Caco-2 and HT-29 cells were counted using a hemocytometer and evenly mixed in a 3:1 ratio(Mingming Zhang *etal* 2022).Both cell lines were purchased in December 2024, and the cells were confirmed to be free from contamination.Both HT-29 and Caco-2 cell lines are derived from colonic adenocarcinoma and exhibit structural and functional characteristics similar to intestinal cells during differentiation. Caco-2 and HT-29 are frequently employed as in vitro models for intestinal epithelial cells and goblet cells **(**Ferraretto *etal* 2018**)**. Although Caco-2 resembles human intestinal epithelial cells morphologically and functionally, numerous reports indicate that Caco-2 cannot produce mucins, to improve the Caco-2 cell model, this study employed co-cultures of mucus-secreting HT-29 cells with Caco-2 cells to model of the human intestine. HT-29 cells secrete multiple mucins, producing mucus similar to that of the human intestinal mucosa.

2.2 Transmission Electron Microscopy (TEM)

Cells were digested with trypsin, centrifuged, and fixed with 2.5% glutaraldehyde at 4°C for 4 hours. Following fixation, the fixative was discarded and samples were rinsed with 0.1 M phosphate-buffered saline (PBS, pH 7.2) for 10 minutes; this rinsing step was repeated four times to thoroughly remove residual fixative. Subsequently, the samples were post-fixed with 1% osmium tetroxide at 4°C for 1–2 hours. After post-fixation, samples were rinsed again with 1× PBS (pH 7.2) for 10 minutes per rinse, repeated three times. The rinsed samples were then dehydrated through a graded ethanol series: 30%, 50%, 70%, 80%, and 90% ethanol (15 minutes per step), followed by two changes of 100% ethanol (10 minutes each). Dehydrated samples underwent resin infiltration and embedding sequentially. They were first treated with an equal-volume mixture of embedding resin and acetone for 1–3 hours. This mixture was then replaced with a 3:1 (v/v) mixture of embedding resin to acetone for a further 3 hours. Finally, samples were infiltrated with pure embedding resin for 12 hours. Following infiltration, embedding was completed through gradient polymerization. The embedded samples were cured using a stepwise thermal protocol: 37°C for 12 hours, followed by 45°C for 12 hours, and a final cure

at 60°C for 48 hours. The cured blocks were first sectioned to obtain semi-thin sections for orientation. Ultrathin sections (70–100 nm in thickness) were then cut using an ultramicrotome. These sections were double-stained by first staining with a 2% uranyl acetate solution for 5–15 minutes, followed by staining with a lead citrate solution for 5–15 minutes. The stained ultrathin sections were examined, and ultrastructural analysis was performed using a transmission electron microscope.

2.3 Western blot (WB)

Protein extraction from treated cells (Bestbio, China) was followed by quantification with a BCA protein assay kit (TianGen, China). Proteins were separated on a SDS-PAGE gel (10% separating gel, 5% stacking gel) and electrophoresed at 80V for 30 min and then 100V for 1 h in 1x running buffer. They were then transferred to a methanol-activated PVDF membrane at 100V using a standard wet transfer method. The membrane was blocked with 5% non-fat milk for 2 h, probed with primary antibody at 4°C overnight, and then with an HRP-conjugated secondary antibody for 2 h at room temperature. After thorough TBST washes, signals were detected with the Electrophoresis Image Analysis System (Shanghai Peiqing Science & Technology Co., Ltd., China). β-actin was used as a loading control. Primary antibodies include: MUC2 (cat. no. ab90007; 5 μg; Abcam), GCNT3(bs-13317R; 50 μl ; Bioss), GCNT1(bs-12334R; 50 μl; Bioss), B3GNT6(21291-1-AP; 50 μl; proteintech), Galnt3(bs-16219R; 50 μl; Bioss), β-actin(8457T; 20 μl; Cell Signaling), Claudin(4933T 20 μl; Cell Signaling), E-cadherin(A20798; 50 μl; ABclonal), Occludin(bsm-60763M; 50 μl ; Bioss), ZO-1(ab276131; 10 μl; Abcam), O-GlcNAcylation (NBP2-59385; 25 μg; Novus), O-GalNAcylation(NBP2-59309; 25 μg; Novus). Secondary antibodies include: Goat anti-Mouse IgG HRP(19z2345; 500 ul; affbiotech), Goat anti-Rabbit IgG HRP (58j9958; 500 ul; affbiotech), Goat anti-Mouse IgM HRP (M212148S; 100 ul; abmart).

2.4 Immunofluorescence (IF)

Cells were seeded in 20 mm glass-bottom dishes (801001; NEST), fixed with 4% paraformaldehyde at 4°C for 30 minutes, and permeabilised with 0.1% Triton X-100 at room temperature for 30 minutes. After blocking in blocking buffer for three hours, the cells were incubated overnight with primary antibodies. This was followed by incubation with fluorescent secondary antibodies. Nuclei were stained with DAPI at room temperature for 5 minutes. Images were acquired using laser confocal microscopy (Nikon, USA). Primary antibodies included: MUC2 (cat. no. ab90007; 5

μg; Abcam), Claudin (4933T 20 μl; Cell Signalling), E-cadherin (A20798; 50 μl; ABclonal), Occludin (bsm-60763M; 50 μl; Bioss), ZO-1 (ab276131; 10 μl; Abcam), O-GlcNAc (NBP2-59385; 25 μg; Novus), and O-GalNAc (NBP2-59309; 25 μg; Novus). Secondary antibodies included: Goat anti-Mouse IgG HRP (19z2345; 500 μl; Affbiotech), Goat anti-Rabbit IgG HRP (58j9958; 500 μl; Affbiotech), and Goat anti-Mouse IgM HRP (M212148S; 100 μl; Abmart).

2.5 Real-time PCR

RNA was extracted from the treated cells using an RNA extraction kit (TIANGEN; CHINA). After quantifying the concentration, the RNA was reverse-transcribed into cDNA using a reverse transcription kit (TIANGEN; CHINA) and stored stably at -80°C. Primers were designed using Primer 5.0 software, as listed in Table 1. The reaction mixture was prepared by sequentially adding the following reagents into each well of an eight-tube strip: 10 μL of UltraSYBR Mix, 1 μL of forward primer, 1 μL of reverse primer, 2 μL of cDNA template, and 6 μL of ddH_2O. After adding all components, the tubes were capped, vortexed thoroughly, and centrifuged. This mixing and centrifugation step was repeated twice. Since the dye is light-sensitive, this procedure should be performed under light-protected conditions. Additionally, contact with the inner surfaces of the tube walls and caps should be avoided during handling. The amplification was then carried out under the following conditions: initial denaturation at 95°C for 10 min; 35 cycles of denaturation at 95°C for 15 s, and annealing/extension at 60°C for 1 min; followed by a final extension at 72°C for 5 min.

Table-1 qPCR primer sequence

Item	GenBank AccessionNo.	Nucleotide sequence of primers (5′- 3′)	Size, bp
GalNT3	NM_052993.3	F:AATCAACCCGATACCAAGT R:TTACAGAATGCTGCCAATG	109
MUC2	XM_054378717	F:ACCAGTAAGTCGTCCTGATCC R:TCGGCCAAATCTTCTCACTCC	128
STIM1	HGNC:11386	F:ATGTATGCGTCCGTCTTGC R:CAATTCGGCAAAACTCTGCT	150
ORAI1	NM_84876	F:GGACGCTGACCACGACTAC R:GGGACTCCTTGACCGAGTT	164
IP3R1	NM_3708	F:GCGGAGGGATCGACAAATGG R:TGGGACATAGCTTAAAGAGGCA	133
IP3R3	NM_002224	F:AGTTCCTGACGTGTGACGAG R:TGAAGCGGTACAAGCCATTCC	171
β-actin	NM_007393.5	F:GTGACGTTGACATCCGTAAAGA R:GCCGGACTCATCGTACTCC	245

2.6 siMUC2

Prior to MUC2 silencing, the cell culture medium was replaced with serum-free medium, and cells were incubated for 24 hours. Subsequently, serum-free Dulbecco's Modified Eagle Medium (DMEM) was mixed with MUC2 small interfering RNA (siRNA), and separately, serum-free DMEM was mixed with a liposomal transfection reagent. After standing for three minutes, the two mixtures were combined and incubated for 20 minutes to form the liposome-nucleic acid transfection complex. After cell washing, the complex was added to the cells. After 6 hours of transfection, the liquid was discarded and replaced with fresh medium. After 48 hours of culture, total RNA was extracted from the cells and subjected to PCR analysis. Silencing efficiency was determined by comparing the negative control, control, and silencing groups. The MUC2 siRNA primer sequences were as follows: forward, 5′-GGAACAUGCAGA AGAUCAATT-3′ and reverse, 5′-UUGAUCUUCUGCAU GUUCCTT-3′ .

2.7 Overexpression of GalNT3

Plasmids were purchased from HENHENG Biotechnology, Inc. and Hieff trans-liposomal transfection reagent was purchased from YENSEN Biotechnology, Inc. Serum-free DMEM-H medium was mixed with the liposomal transfection reagent and plasmid (liposomal transfection reagent: plasmid = 3:1). DNA (2 μg) was added to 250 mL of serum-free culture medium, followed by the transfection reagent. The preparation was kept for 3 min. The diluted DNA and liposomal transfection reagent were gently mixed and incubated at room temperature for 20 min to form the DNA–liposome complex. For cell transfection, Caco-2 and HT-29 cells in a 3:1 ratio were seeded in 6-well plates at a density of 1×10^5 cells/cm^2 before transfection. The cells were then transfected upon reaching a 90% to 95% confluency in antibiotic-free medium. The DNA-Hieff Trans™ complex was added to each well of the cell culture plate, followed by incomplete DMEM-H medium to a total volume of 2 mL. The culture plates were shaken gently. After 6 h of incubation at 37°C in a 5% CO_2 atmosphere, the growth medium was replaced. After 48 h of culture, RNA was extracted, and the expression of GalNT3 and MUC2 genes in the transfection and LPS(-) groups was detected using fluorescence quantitative PCR. For challenged cells after transfection (LPS(+)+overexpression [OE] group), the culture medium was changed to 1.5 mL of medium containing 400 μg/mL after 6 h, and incubation was continued for 48 h.

2.8 Fast and comprehensive O-glycoproteomics analysis with MSFragger-Glyco

2.8.1 Protein extraction

Samples were removed from storage at -80°C, and each group of samples was lysed by adding a 4-fold volume of lysis buffer (8 M urea, 1% protease inhibitor, 3 μM TSA, and 50 mM NAM), followed by ultrasonication. The cellular debris was removed, the supernatant was transferred to a new centrifuge tube, and the protein concentration was determined using a BCA kit.

2.8.2 Trypsin digestion

An equal amount of each sample protein was taken for enzymatic digestion. The lysate volume was adjusted to consistency, and TCA was slowly added to a final concentration of 20%, with vortexing and mixing, and the precipitate was allowed to settle at 4°C for 2 h. After drying the precipitate, 200 mM tetraethylammonium bromide was added, sonicated to break up the precipitate. Trypsin was added at a ratio of 1:50 (protease:protein, m/m) and digested overnight. Iodoacetamide was then added to a final concentration of 11 mM, and the solution was incubated for 15 min at room temperature in the dark.

2.8.3 Modification enrichment

The peptide was dissolved and added to a RAX column. The eluted peptide was then obtained and drained for quantification according to the manufacturer's instructions. The eluted intact glycopeptide was dissolved in PBS (pH 7.4), and the supernatant was transferred to the AminoLink resin and mixed with NaBH3CN at a final concentration of 50 mM for overnight incubation. At the end of the incubation, the eluted glycopeptide was sequentially incubated with 50% acetonitrile, 1.5 M NaCl, and 20 mM Tris-HCl (pH 6.8) three times to wash the resin. Finally, O-glycoprotease was added and digested overnight at 37°C to elute the resin-bound peptides. The combined eluates were collected and freeze-dried under vacuum. After extraction and desalting using C18 ZipTips, the resin was freeze-dried under vacuum and analysed using liquid chromatography (LC)–mass spectrometry. The peptides were separated using ultra-high-performance LC, injected into an NSI ion source for ionisation, and then analysed using Orbitrap Astral mass spectrometry(Detailed experimental procedures are shown in Supplementary-1).

2.9 Co-immunoprecipitation (co-IP)

Cells were harvested, rinsed with PBS, and lysed on ice using a lysis buffer comprising multiple constituents to liberate the proteins. For IP, the lysate was retrieved,

and specific antibodies were incorporated, followed by incubation overnight at 4°C with gentle stirring to allow immune complex formation. Thereafter, depending on the antibody classification, Protein A or G agarose beads were added and incubated at 4°C for several hours. The complexes were recovered by centrifugation and washed repeatedly with pre-cooled washing buffer to eliminate impurities and unbound proteins, and decrease non-specific binding. The bound proteins were then eluted by adding an elution buffer. Western blotting, mass spectrometry, and other techniques were used to assay the eluted proteins. Western blotting allows the detection of specific proteins and estimation of their molecular weight and relative quantity using specific antibodies. Mass spectrometry comprehensively identifies protein varieties, thereby identifying proteins that interact with the target protein.

2.10 Prediction of protein-protein interactions

The predicted structure of P12830 (CADH1_HUMAN) was acquired from the UniProt database as an AlphaFold2-generated PDB file, while a specific 2,000-amino acid segment of Q02817 (MUC2_HUMAN) was modeled using SWISS-MODEL. Subsequently, protein-protein docking between these two structures was performed using the ClusPro server with default parameters for global docking, which generated an ensemble of predicted complex models. Finally, the resulting docked complexes were visualized and analyzed using PyMOL.

2.11 Measurement of Intracellular Calcium Ion Concentrations

Intracellular calcium ion concentration was measured using the fluorescent indicator Indo-1/AM (Yeasen, China). Briefly, a 5 mM stock solution was prepared by dissolving Indo-1/AM in DMSO, which was then diluted in PBS to a 5 μM working solution. Cells were washed three times with PBS and incubated with the working solution at 37°C for 45 minutes. After loading, cells were washed three times with PBS to remove extracellular dye and covered with fresh PBS. Fluorescence intensities were measured simultaneously at 400 nm and 475 nm (emission) under 346 nm excitation using a fluorescence microplate reader. The calcium ion concentration was calculated based on the ratio of fluorescence intensities (F400/F475).

2.12 RNA-seq

Total RNA was extracted from control group, LPS group, oe-GalNT3 group and LPS+oe-GalNT3 group using RNA extraction kits. We used the Illumina TruSeq Stranded Total RNA Library Prep kit to generate an RNA-seq library according to the

manufacturer's protocol, and high-throughput sequencing was then performed on an Illumina HiSeq 2500 system. RNA-seq data were processed through a computational pipeline. The original data were compared with the human genome, and differentially expressed genes were selected based on the criteria of fold change> 2 and false discovery rate < 0.05.

2.13 Statistical analysis

Statistical analyses were performed using GraphPad Prism (version 7) and the Statistical Package for Social Sciences (SPSS). Continuous data are presented as the mean ± standard deviation. Differences between the test group and control groups at various time points were assessed using one-way analysis of variance (ANOVA) followed by Tukey' s post hoc test. A P value of less than 0.05 was considered statistically significant.

3.Results

3.1 Effects of LPS on glycosyltransferases during O-glycan formation in MUC2

To analyse the effect of LPS on the O-glycosylation of MUC2, we first confirmed the changes that occurred during the MUC2 synthesis process. We cultured Caco-2/HT29 cells and evaluated their responses at 24, 36, 48, and 72 h after LPS treatment. MUC2 secretion was the highest at 36 h in both the LPS(-) and LPS(+) groups, effectively preventing LPS translocation into cells. This was verified using epifluorescence microscopy, which showed markedly reduced fluorescein isothiocyanate (FITC)-LPS levels within the cells (Figure 1A). At this time point, MUC2 expression in both the LPS(-) and LPS(+) groups began to decline, and LPS translocation into cells increased with the reduction of MUC2 from 48 to 72 h. These data demonstrate that MUC2 plays a primary role in defending against LPS translocation.

MUC2 expression was significantly decreased in the LPS(+) group compared with that in the LPS(-) group at 72 h ($P < 0.05$). Meanwhile, the expression of GalNT3 and B3GNT6 in the LPS(+) group was significantly decreased compared with that in the LPS(-) group at 72 h ($P < 0.05$). No significant difference in GCNT1 and GCNT3 expression was found between the LPS(-)and LPS(+) groups ($P > 0.05$) (Figures 1C and 1D). This result indicates that MUC2 expression follows the same trend as that of GalNT3 and B3GNT6 expression.

The results of transmission electron microscopy (TEM) showed that after 24 h of

LPS treatment, small vacuoles appeared around the mucin granules in the cytoplasm (red arrow). At 36 hours, extensive swelling of the endoplasmic reticulum (ER) was observed in the cytoplasm (red boxes). By 48 hours, the number of small vacuoles around the mucin granules in the cytoplasm further increased (green box). After 72 hours, the ER swelled more severely and became rounded (green arrow and blue box), accompanied by numerous small vacuoles and severe damage to the cellular structure (Figure 2B).

We therefore speculate that LPS primarily inhibits the initial phase of MUC2 O-glycosylation modification in the endoplasmic reticulum.

3.2 Effects of GalNT3 and siMUC2 overexpression on tight junction proteins following LPS treatment

We aimed to enhance the post-translational modification and production of MUC2 by overexpressing the key glycosyltransferase GalNT3. We transfected an overexpression plasmid for GalNT3 into Caco2/HT29 cells after 72 h of LPS treatment. This led to GalNT3 overexpression, which resulted in significantly increased mRNA and protein levels of both GalNT3 and MUC2 after LPS treatment (Figure 2-1B). Meanwhile, silencing the MUC2 gene significantly decreased MUC2 mRNA and protein expression compared with those in the LPS(-) group in Caco2/HT29 cells at the same time point (Figure 2-1A).

ZO-1 protein expression was significantly decreased in the siMUC2+LPS group compared with that in the LPS(-) group ($P < 0.05$). Claudin protein expression in the siMUC2+LPS and LPS groups was higher than that in the oe-GalNT3+LPS and LPS(-) groups ($P < 0.05$). The JAMA levels did not differ significantly among the oe-GalNT3+LPS, LPS(+), LPS(-), and siMUC2+LPS groups ($P > 0.05$). E-cadherin protein expression in the oe-GalNT3+LPS group was significantly higher than in the LPS(+) and siMUC2+LPS groups ($P < 0.05$). The occludin protein expression in the oe-GalNT3+LPS group was significantly increased compared with that in the siMUC2+LPS group ($P < 0.05$) (Figure 2-2C).

E-cadherin and MUC2 expression in the LPS(+) group were significantly lower than those in the LPS(-) group, and cell-to-cell connectivity was looser. Large spaces were evident between cells. Further, MUC2 expression and the number of cells in the siMUC2+LPS group were lower than those in the LPS(-) group, and cell-to-cell connectivity was looser, with larger spaces between cells. In contrast, the oe-GalNT3+LPS group showed increased overlap between E-cadherin and MUC2;

further, the high levels of MUC2 increased the E-cadherin protein expression, which aggregated the cells and caused them to tightly connect and form clusters (yellow box in Figure 2-2D).

MUC2 overexpression did not promote ZO1 and Claudin protein expression (Figure 2-3E). Although occludin and MUC2 proteins showed similar trends, the overlap between the two proteins was very low. When MUC2 was abundantly secreted, it adhered to the E-cadherin protein, which could effectively reduce the damage evident in the LPS(+) and LPS+siMUC2 groups (Figure 2-2D). Subsequently, the oe-GalNT3 group showed higher expression of MUC2 and E-cadherin protein compared with that in the LPS group ($P < 0.05$), with no significant difference in MUC2 and E-cadherin protein expression between the oe-GalNT3+LPS and LPS(-) groups ($P > 0.05$) (Figure 2-3F).

Therefore, these results suggest that overexpression GalNT3 induced the secretion of large amounts of MUC2. This secreted MUC2 could adhere to and interact with E-cadherin, leading to cell aggregation and cluster formation, ultimately enhancing cell density after LPS treatment.

3.3 The interaction between MUC2 and E-cadherin after LPS treatment

To determine whether MUC2 and E-cadherin interact upon LPS treatment, we performed immunoprecipitation (IP) to purify these proteins from total cell lysates. The results confirmed a strong interaction between MUC2 and E-cadherin by co-IP (Figure 3A). Furthermore, analysis of the predicted protein structure of E-cadherin (UniProt ID: P12830) indicated that its N-terminal region (amino acids 0–500) interacts with the central region (amino acids 1000–1500) of MUC2. The interacting interface is highlighted in blue (Figure 3B).

3.4 Effects of LPS on O-glycan chain structure of MUC2 in Caco2/HT29 co-culture cells

To further elucidate the repair function of MUC2 on E-cadherin after LPS treatment in Caco-2/HT29 cells, we used *MSFragger-Glyco* to analyse O-glycosylation in MUC2. Among these, 48 and 135 intact glycopeptides (IGPs), 39 and 84 proteins, and 42 and 114 sites were up-regulated and down-regulated, respectively. These results confirm that the O-glycan chain structure of glycoprotein changed significantly after LPS treatment (Figure 4-1 A). The O-glycan changes in these glycoproteins were mainly concentrated in the Sia, HexNAc, Fuc, and Hex glycan chains (Figure 4-1B). The result showed two O-glycans per glycosite in 97

glycopeptides, one O-glycan per glycosite in 440 glycopeptides, two glycosites per protein in 68 glycopeptides, and one glycosite per protein in 205 glycopeptides (Figure 4-1C). Among these glycoproteins, the mucins MUC2, MUC5AC, and MUC13 showed significant changes in O-glycan structure (Figure 4-1D).

O-glycosite structural changes were evident in MUC5AC, MUC2, and MUC13 among mucins, with changes in MUC2 being even more prominent. Six sites (46T, 46T, 56T, 68S, 84T, and 167T) were newly added with HexNAc(5), HexNAc(6), HexNAc(2)(Core-3), HexNAc(1)Hex(3)Fuc(1), HexNAc(2)(Core-3), and HexNAc(1) in MUC2 at the O-glycosite structure in the LPS(+) group, respectively.

The O-glycosite abundance of 57T-HexNAc(1), 68S-HexNAc(1), 84T-HexNAc(1), 147T-HexNAc(5), 170S-HexNAc(2), and 171T-HexNAc(1) in MUC2 was significantly lower in the LPS(+) group compared with that in the LPS(-) group. The 67T-HexNAc(2)(Core-3), and 108S-HexNAc(4), 117T-HexNAc(5), and 166S-HexNAc(2) were lost from MUC2 in the LPS(+) group (Figure 4-2A).

In summary, these results demonstrate that the long O-glycan chains of MUC2 are lost and show significantly lower abundance of HexNAc-containing O-glycan chains attached to threonine (Thr) residues after LPS treatment.

3.5 Effects of LPS on O-glycosylation modifications of MUC2 and E-cadherin

The term HexNAc mainly refers to two monosaccharides: GalNAc and GlcNAc, which are components of O-glycans. The two most common types of O-linked glycosylation are O-linked-acetylgalactosamine (O-GalNAc) and O-linked-β-D-N -acetylglucosamine (O-GlcNAc).

We subsequently isolated and purified both MUC2 and E-cadherin proteins (Figure 5A). We further analysed the O-GlcNAc and O-GalNAc levels in purified MUC2 and E-cadherin proteins in LPS(-), LPS(+) group. The results showed that O-GlcNAc in MUC2 of the LPS(-) group was significantly increased compared with that in the LPS(+) group, and O-GlcNAc in E-cadherin of the LPS(-) group was not significantly different compared with that in the LPS(+) group ($P > 0.05$). O-GalNAc in MUC2 and E-cadherin of the LPS(-) group was significantly increased compared with that in the LPS(+) group ($P < 0.05$), the change of O-GalNAc in MUC2 was even more noticeable (Figure 5C).

The colocalisation of both O-GlcNAc and O-GalNAc with MUC2 and E-cadherin was nearly consistent between the LPS(-) and LPS(+) groups. LPS did not exert a significant effect on O-GlcNAc, whereas it markedly reduced the level of

O-GalNAc in E-cadherin and MUC2 as observed in the LPS(+) and LPS(-) groups ($P < 0.05$). O-GalNAc could enhance the adhesion link structure between cells; further, the distribution of O-GalNAc, E-cadherin, and MUC2 was merged in Figure 5B.

These findings suggested that LPS mainly affects O-GalNAc of MUC2 and E-cadherin, and that O-GalNAc induces increased MUC2 and merging of E-cadherin and MUC2. Overall, O-GalNAc exerts a strong effect on MUC2 after LPS treatment.

3.6 Changes in the O-glycan chain structure of MUC2 and E-cadherin following LPS treatment and GalNT3 overexpression

The Tn antigen structure is formed by GalNAc transferase (GalNT3) attaching GalNAc to Ser/Thr to complete GalNAcylation. Further, LPS primarily inhibits the initial phase of O-glycosylation in MUC2. Therefore, we continued to overexpress GalNT3 in the cells.

The results showed that 67T-HexNAc (5), 67T-HexNAc (2) (Core-3), 102T-HexNAc (5), 102T-HexNAc (6), 102T-HexNAc (4), 117T-HexNAc (4), 117T-HexNAc (5), 117T-HexNAc (6), 138T-HexNAc (1), 138T- HexNAc (2) (Core-3), 147T-HexNAc (5), 147T-HexNAc (4), and 166S-HexNAc (2) (Core-3) of MUC2 in the oe-GalNT3+LPS group were newly added compared to those in the LPS(+) group.

Further, O-glycan abundance of 35T-HexNAc(1), 46T-HexNAc(1), 57T-HexNAc(1), 67T-HexNAc(3)(Core-4), 68S-HexNAc(1), 84T-HexNAc(1), 84T-HexNAc(3) (Core-4), and 170T-HexNAc(1) in MUC2 was higher in the oe-GalNT3+LPS group than in the LPS(+) group.

Four O-glycans, HexNAc(6), HexNAc(1), HexNAc(4), and HexNAc(2) (Core-3) at sites 46T, 97T, 108S, and 56T of MUC2 in the oe-GalNT3+LPS group were lost compared with those in the LPS(+) group, respectively. Further, O-glycan abundance of 46T-HexNAc(5), 67T-HexNAc(4), 167T-HexNAc(1), 170S-HexNAc(2), and 171T-HexNAc(1) of MUC2 in the oe-GalNT3+LPS group was lower than that in the LPS(+) group (Figure 6-1A).

Further, 646T-HexNAc(1) in E-cadherin from the oe-GalNT3+LPS group was newly added compared with that in the LPS(+) group; 509-HexNAc(1) and 646-HexNAc(1) in E-cadherin from the LPS(+) group were lost compared with those in the LPS(-) group (Figure 6-1B).

These results suggested that in the oe-GalNT3+LPS group, MUC2 had acquired new O-glycans and showed up-regulated long-chain O-glycan abundance; these

newly added glycans were primarily of the HexNAc subtypes. Up-regulation of O-GalNAc can increases the length of MUC2 O-glycan chains, promoting the extension of MUC2 O-glycan chains and the reconstruction of the O-glycan backbone, thereby enhancing the integrity of the mucus layer.In contrast, the O-glycan structure of E-cadherin showed almost no changes in the oe-GalNT3+LPS group.

3.7 MUC2 repairs E-cadherin through Adherens junction

Based on our previous analysis of *MSFragger-Glyco* results, comparisons between the LPS+oeGalNT3 *vs.* LPS(+) groups and LPS(-) *vs.* LPS(+) groups revealed that at the KEGG mapping level, the most significantly enriched pathways in the LPS+oeGalNT3 group were ECM-receptor interaction, Protein processing in the endoplasmic reticulum, and Adherens junctions, relative to the LPS(+) group. In the Domain dot plot, the main enrichment was found in the Calcium-binding EGF domain when comparing both the LPS *vs.* LPS+oeGalNT3 groups and the LPS(-) *vs.* LPS(+) groups (Figure 7 A, B).

In the Adherens junction pathway, the stronger adhesion between E-cadherin on the neighbouring cell membrane was due to the presence of Ca^{2+} ions; without Ca^{2+} ions, the adhesion between E-cadherin on neighbouring cell membranes was weak. We further found that the Ca^{2+} concentration in the oeGalNT3 group was higher than that in the LPS+oeGalNT3 group, which in turn was higher than that in the LPS(-) group, and this was higher than that in the LPS(+) group (Figure 7C).

The enzyme activity of Ca^{2+}-ATP in the oe-GalNT3 group was significantly higher than that in the oe-GalNT3+LPS and LPS groups (P<0.05) (Figure 7E). ST1M1 and Orai1 mRNA expression in the oe-GalNT3 group was significantly higher than that in the oe-GalNT3+LPS, control, and LPS groups (P<0.05). The expression of IP3R1 and IP3R2 mRNA in the oe-GalNT3 group was significantly higher than that in the oe-GalNT3+LPS and LPS groups (P<0.05) (Figure 7G**)**. PMCA4 protein expression in the oe-GalNT3 group was significantly higher than that in the oe-GalNT3+LPS and LPS groups (P<0.05); further, SERCA2b protein expression in the oe-GalNT3 group was significantly higher than that in the oe-GalNT3+LPS, control, and LPS groups (P<0.05) (Figure 7F**)**.

In further, we assessed the barrier function of clustered cells on FITC-LPS translocation. Under normal conditions, MUC2 can form a good barrier in the mucus layer, allowing it to invade cells that contain less LPS. In these samples there was a low green positive signal was observed (Figure 7H). Over-expression of GalNT3 in

cells thickened the cellular mucus layer composed of MUC2, which effectively blocked LPS translocation into cells, as evidenced by nearly negligible green fluorescence.

These results indicate that up-regulation of O-GalNAc can aslo activate the Adherens junction pathway and Calcium-binding EGF domain. O-GalNAc glycosylation also enhances the function of calcium-binding proteins, thereby promoting intracellular Ca^{2+} concentrations and strengthening E-cadherin-mediated intercellular adhesion junctions. Consequently, MUC2 restores the barrier function of the mucus layer through O-GalNAc glycosylation, promotes Ca^{2+} absorption and enhances E-cadherin-mediated adhesion junctions; the combined action of double barrier function of the intestinal mucosal epithelium, thereby preventing the invasion of endotoxins.

3.8 Effect of GalNT3 Overexpression on the Expression of HexNAc Glycan Chains on Calcium-Regulated Factors after Treatment LPS

Analysis of glycan changes in previously identified cells revealed 14 genes with significant variations in HexNAC glycan profiles associated with calcium ions: AGRN, NUCB1, CANX, LDLR, CXCL16, CD44, PLXNB1, ERP44, CD320, ASPH, LTBP3, PRKCSH, MAN1B1, and APLP2(Figure 8A and Table-1). Transcriptomics results were used to validate the mRNA expression levels of these 14 genes in the four groups.

The results showed that, CANX, PLXNB1, ERP44, APLP2, AGRN and CD320 mRNA expression in the oe-GalNT3 group were significantly higher than that in the Control group (P<0.05); CANX, PLXNB1, ERP44, APLP2, AGRN and CD320 mRNA expression in the LPS group were significantly lower than that in the Control group (P<0.05); CANX, PLXNB1, APLP2 and ERP44 mRNA expression in the LPS+oe-GalNT3 group were not different compare to control group(P>0.05).NUCB1 and PRKCSH mRNA expression in the oe-GalNT3 group was significantly higher than that in the LPS group, Control group and LPS+oe-GalNT3 group (P<0.05). The LDLR mRNA expression of Control group and oe-GalNT3 group were than that in the LPS group and LPS+oe-GalNT3 group (P<0.05). CD44 mRNA expression in the LPS group was significantly lower than that in the Control group, oe-GalNT3 group and LPS+oe-GalNT3 group (P<0.05) (Figure 8B).

GO functional annotation and KEGG pathway enrichment analysis were performed on 14 genes. The GO analysis results indicated that calcium ion binding

was the most significantly enriched molecular function, observed in 8 of the genes (AGRN, NUCB1, CANX, LDLR, CD320, LTBP3, PRKCSH). MAN1B1 and EPR44 are significantly enriched in glycoprotein metabolic process. In addition, CANX is significantly enriched in the endoplasmic reticulum and protein-binding. LDLP and CD320 are significantly enriched in receptor-mediated endocytosis. LTBP3 is significantly enriched in the collagen-containing extracellular matrix. MAN1B1 is significantly enriched in metal ion binding. CD44 is significantly enriched in positive regulation of heterotypic cell-cell adhesion, cell-matrix adhesion, focal adhesion, cell-cell adhesion, cell surface, and cell adhesion. PLXNB1 is significantly enriched in negative regulation of cell adhesion. ERP44 is significantly enriched in endoplasmic reticulum-golgi intermediate and endoplasmic reticulum lumen. ASPHD2 and PRKCSH are significantly enriched in metal ion binding. APLP2 is significantly enriched in transition metal ion binding and endoplasmic reticulum lumen. KEGG pathway analysis shows AGRN and CD44 are significantly enriched in ECM-receptor interaction. CXCL16 is significantly enriched in Cytokine-cytokine receptor interaction (Figure 8C).

These results indicate that GalNT3 influences the mRNA expression levels of multiple calcium-related genes by regulating their HexNAc glycosylation, thereby participating in various biological processes such as cell adhesion, migration, inflammatory responses, and lipid metabolism.

4.Discussion

LPS is the toxic component of endotoxin and the main component of the outer membrane of Gram-negative bacteria. At high concentrations, LPS causes extensive and intense inflammatory reactions. The intestinal mucus layer, with MUC2 as its core component, constitutes the first line of defence for the mucosal barrier **(**Corfeld *et al.* 2015**)**. In a previous study, we demonstrated that the tight junction structure of cells in areas with MUC2 was not disrupted by LPS. Further, MUC2 (mucin-2) has the highest rate of change compared with that of other mucins after LPS treatment (Dujian *et al.* 2024). However, the pathway through which MUC2 acts to repair tight junction structures remains unclear. In this study, the initial phase of MUC2 O-glycosylation in the endoplasmic reticulum of intestinal epithelial cells was found to be critical for LPS-induced damage. MUC2 monomers are linked by disulfide bonds in the endoplasmic reticulum to form oligomers, which then leave the

endoplasmic reticulum and enter the Golgi **(**Katrine *et al.* 2020; Elizabeta *et al.* 2024**)**. The expression levels of GalNT3 and B3GNT6 proteins in the LPS(+) group were significantly decreased compared with the LPS(-) group. The Tn antigen structure is formed by GalNAc transferase (GalNT3) attaching GalNAc to Ser/Thr in the endoplasmic reticulum. Further, GalNT3 overexpression by plasmid transfection into cells also enhanced MUC2 expression in Caco2/HT-29 cells.

The expression of Occludin and E-cadherin proteins followed the same trend of decreasing and increasing expression alongside MUC2 protein expression. However, only E-cadherin and MUC2 proteins interacted with each other to form denser and more cluster-like cell-to-cell connections, which LPS could not destroy. The expression of E-cadherin and MUC2 proteins in the oe-GalNT3 and oe-GalNT3+LPS groups was higher than that in the LPS(-) and LPS(+) groups. We thus hypothesise that the increase in MUC2 protein promotes E-cadherin protein expression. To test this hypothesis, co-IP and AlphaFold2 were used to confirm the interaction between E-cadherin and MUC2 in Caco2/HT-29 cells.

To further elucidate MUC2 repair function on E-cadherin, the O-glycan chain structure of MUC2 and E-cadherin was measured using *MSFragger*-Glyco analysis **(**Steentoft *et al.* 2013; Joshi *et al.* 2018; Amon *et al.* 2014**)**. LPS treatment resulted in the loss or reduced abundance of most long-chain O-glycans (67T-Core-3, 108S-HexNAc(4), 117T-HexNAc(5), 147T-HexNAc(5), 166S-Core-3, and 170S-Core-3) and an increase in short-chain O-glycans (67-T-Core-4, 84T-Core-4, 97T-HexNAc(1),167T-HexNAc(1), and 170T-HexNAc(1)) on MUC2. This result also showed that glycan subtype changes were mainly enriched in HexNAc (GalNAc and GlcNAc). The two most common types of O-linked glycosylation are O-GalNAc and O-GlcNAc. O-GalNAc glycosylation is initiated by polypeptide N-acetylgalactosaminyl-transferase. GalNAc monosaccharides are attached to the Ser or Thr protein residues by O-glycosidic bonds (Weiyu Li *et al.* 2022; Marsico *et al.* 2018). This dense O-GalNAc glycosylation, also known as mucin-type O-glycosylation, is observed in various tumour types and plays a role in cell-cell and cell-matrix interactions (Goth *et al.* 2017; Goth *et al.* 2018).

Next, we analysed O-GalNAc and O-GlcNAc on purified E-cadherin and MUC2. O-GalNAc of MUC2 and E-cadherin was higher in the LPS(+) group than in the LPS(-) group. O-GlcNAc of E-cadherin did not differ between the LPS(+)and LPS(-) groups. At the more basic structural level, O-GalNAc addition to MUC2 extends its

polypeptide backbone and with increased MUC2 O-glycan density (Larsen *et al.* 2017; Schjoldager *et al.* 2020; Liu *et al.* 2011). We analysed the O-glycan chain structures of E-cadherin and MUC2 in the oe-GalNT3 and oe-GalNT3+LPS groups. GalNT3 overexpression in the LPS(+) group led to the new addition or increased abundance of most long-chain O-glycans (67T-HexNAc(5), 67T-Core-3, 67T-core-4,102T-Hex NAc(5), 102T-HexNAc(6), 102T-HexNAc(4), 117T-HexNAc(5), 117T-HexNAc(6), 117T-HexNAc(4), 138T- Core-3, 147T-HexNAc(5), and 147T-HexNAc(4)) and decreased the short-chain O-glycans (46T-HexNAc(5), 46T-HexNAc(6), 67T-HexNAc(6), 167T-HexNAc(1), 170T-Core-3, and 171T-HexNAc(1)) on MUC2 compare with the LPS(+) group. However, the O-glycan chains of E-cadherin were almost unchanged after GalNT3 overexpression in the LPS(+) group. There is a significant increase in O-GalNAc glycosylation of the MUC2 protein after overexpression GlaNT3. This upregulation of O-GalNAc glycosylation enhances the long-chain O-glycan structure of MUC2, repairs the O-glycan backbone and the barrier function of the mucin layer, and protects the underlying epithelial cell junctions.

E-cadherin, a group of transmembrane glycoproteins, is a class of Ca^{2+}-dependent homophilic cell adhesion molecules responsible for facilitating cell-cell adhesion (Goettig *et al.* 2016; Steentoft *et al.* 2013). Whether treated with LPS or oe-GalNT3 in cells, O-glycopeptide KEGG pathway enrichment was observed in the Calcium-binding EGF domain. However, the new addition of long O-glycan chains and the rising abundance of original O-glycan chains from MUC2 in oe-GalNT3+LPS group were newly enriched in the adherens junction signalling pathway. This demonstrated that enhanced O-GalNAc could activate the Adherens junction signalling pathways**(**Pinto *et al.* 2023**)**. E-cadherin—a class of Ca^{2+}—dependent heterophilic cell adhesion molecules—can specifically recognise and adhere to specific glycosyl groups in oligosaccharide chains on the surface of other cells, mediating intercellular recognition and adhesion (Gupta *et al.* 2020; Ten Hagen *et al.* 2001; Bergstrom *et al.* 2013; Schjoldager *et al.* 2012). O-GalNAc sufficiency primarily affects the glycosylation of calcium-related and cell adhesion-related proteins, supporting calcium signaling and compromising cell adhesion(Rui Ma *et al.*2026). STIM1 is the “sensor” for calcium depletion in calcium stores and a key molecule activating Orai channels. STIM1 is a widely expressed regulator of basal calcium levels and a facilitator of receptor-operated calcium influx

(Philip *et al.* 2022**)**. IP3R1/2/3 (Inositol trisphosphate receptors) mediate IP3-dependent calcium release from the endoplasmic reticulum **(**Fatma *et al.* 2024**)**. The primary plasma membrane calcium ATPase (PMCA4) in HT29 cells is responsible for pumping Ca^{2+} from the cytoplasm to the extracellular space **(**Zhang *et al.* 2020**)**. SERCA2b shows relatively high calcium affinity, enabling Ca^{2+} uptake from the cytoplasm into the endoplasmic reticulum. Transcriptomic results indicate the HexNAc glycan chains on Calcium-regulated factors expression in LPS+oe-GalNT3 group were not different compare to LPS group. Base on these findings, we propose that over-expression GalNT3 can restore the O-GalNAc glycosylation of calcium-related and adhesion-renlated proteins, leading to regulated calcium signaling and cell adhesion, which ultimately repair in intestinal barrier function (Rui Ma *et al.* 2026) (Figure-9).

This study addresses several critical gaps in the field. Firstly,we demonstrated that LPS induces damage to the endoplasmic reticulum, affecting the initiation site of the O-glycosylation synthesis process. LPS causes significant changes on the O-glycan structure of MUC2, with a loss of long-chain O-glycans and the additional of short-chain O-glycans; the HexNAc glycan type exhibits the most changed; however, the O-glycan chain structure of E-cadherin was fewer alterations. Secondly, overexpression of GALNT3, O-GalNAcylation of the MUC2 protein increased significantly. Upregulation of O-GalNAc glycosylation enhances the long-chain O-glycan of MUC2, repairs the O-glycan backbone structure and the barrier function of the mucin layer, and protects the underlying epithelial cell junctional structures. Thirdly, the upregulation of O-GalNAcylation also enhances the function of Calcium-related proteins, promotes intracellular Ca^{2+} concentration, and strengthens E-cadherin-mediated intercellular junctions.

In summary, The dual actions of remodelling of MUC2 O-glycan structure and the reinforcement of E-cadherin junctions together reduced the cellular injury caused by LPS translocation.These findings not only advance our understanding of the molecular mechanisms underlying intestinal barrier biology but also offer novel perspectives for developing therapeutic interventions targeting intestinal barrier-related diseases.

Figure

Figure 1. Effect of LPS on barrier function and O-glycosylation of MUC2 in Caco2/HT-29 cells. A. Effect of LPS on the barrier function mediated by MUC2 at 24 h, 36 h, 48 h, and 72 h. **B,** Enlargement of the endoplasmic reticulum of cells observed using TEM after LPS treatment for 24 h (red arrow) and 36 h (red box). Fat droplets on cells after LPS treatment for 48 h (green box). Cellular swelling (blue box) and fat droplets (green arrow) on cells after LPS treatment for 72 h. **C, D**, Effects of LPS on O-glycosyltransferase expression in cells at 24 h, 36 h, 48 h, and 72 h.

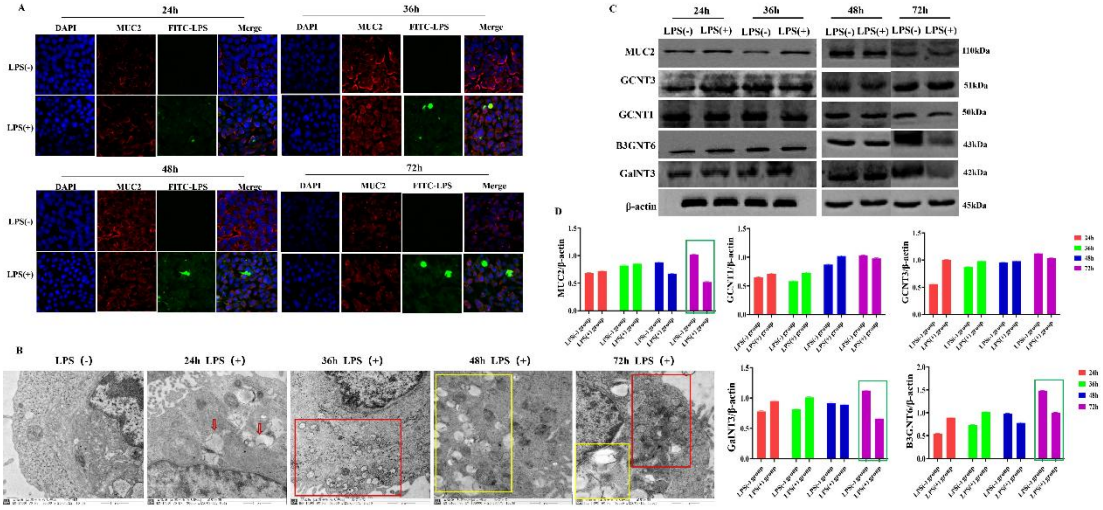


Figure 2 Changes in tight junction and adhesive junction protein expression and their distribution in LPS(-), LPS(+), oe-GalNT3+LPS, and siMUC2+LPS groups. A, MUC2 mRNA and protein expression in the negative control, siMUC2+LPS, and control groups. B, mRNA and protein expression of GalNT3 and MUC2 in the negative control, oe-GalNT3+LPS, and control groups. C, Changes in the tight junction and adhesive junction proteins in the LPS(-), LPS(+), oe-GalNT3+LPS, and siMUC2+LPS groups. D, Distribution of E-cadherin and Occludin proteins observed by fluorescence microscopy in the LPS(-), LPS(+), oe-GalNT3+LPS, and siMUC2+LPS groups (DAPI, fluorescent blue; E-cadherin and Occludin, fluorescent green; MUC2, fluorescent red). E, Distribution of Claudin and ZO-1 proteins observed by fluorescence microscopy in the LPS(-), LPS(+), oe-GalNT3+LPS, and siMUC2+LPS groups (DAPI, fluorescent blue; Claudin and ZO-1, fluorescent green; MUC2, fluorescent red). F, The protein expression of E-cadherin and MUC2 in the LPS(-), LPS(+), oe-GalNT3+LPS, and oe-GalNT3 group.

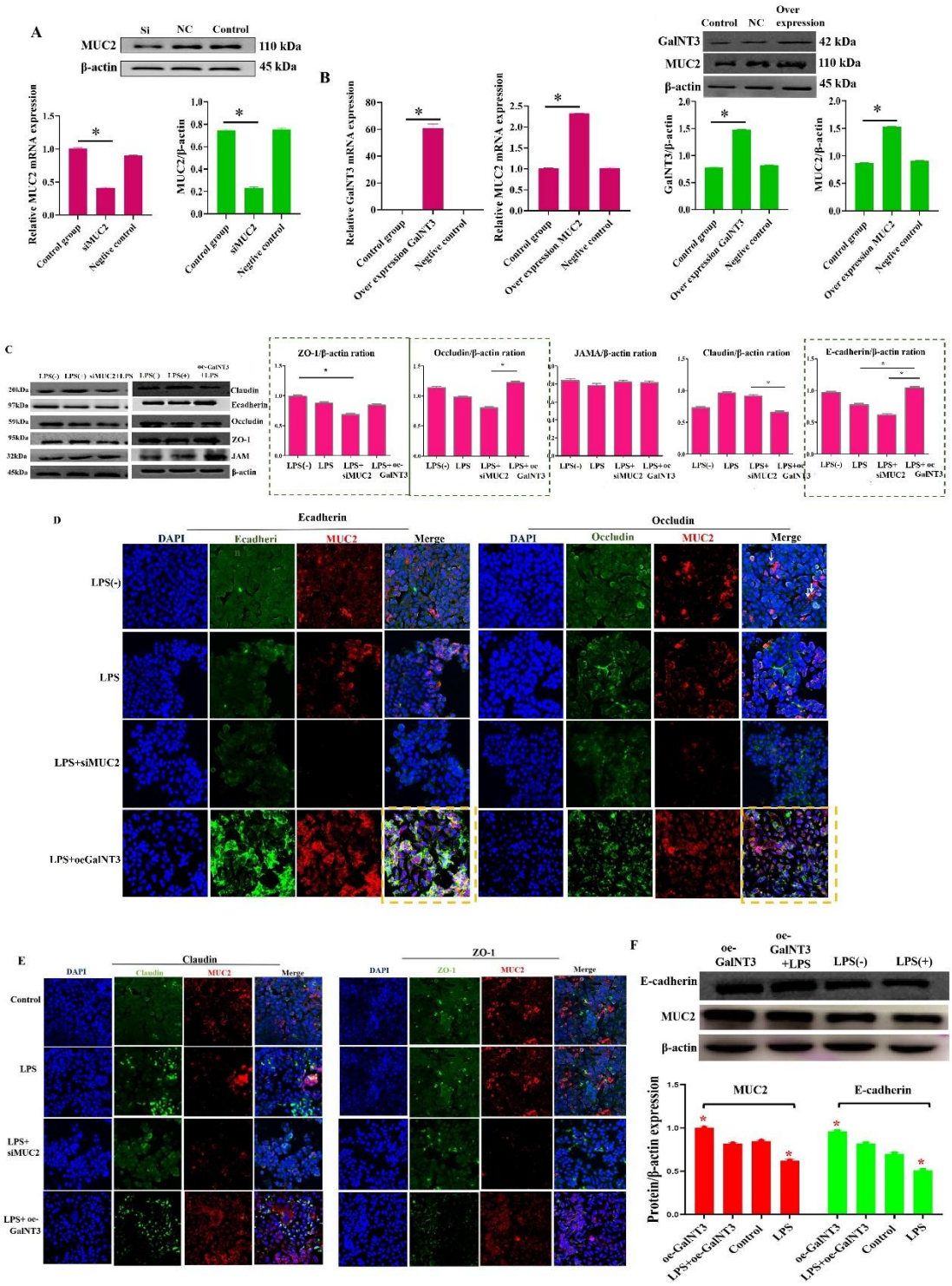


Figure 3 Interaction between E-cadherin and MUC2. A, Protein E-cadherin and MUC2 were purified using immunoprecipitation, Co-IP analysis of interaction between E-cadherin and MUC2 in cells. B, Predicted protein structure of the N-terminal region (amino acids 0–500) of E-cadherin interacts with a central region (amino acids 1000–1500) of MUC2. The interacting interface determined using SWISS-MODEL analysis is highlighted in blue.

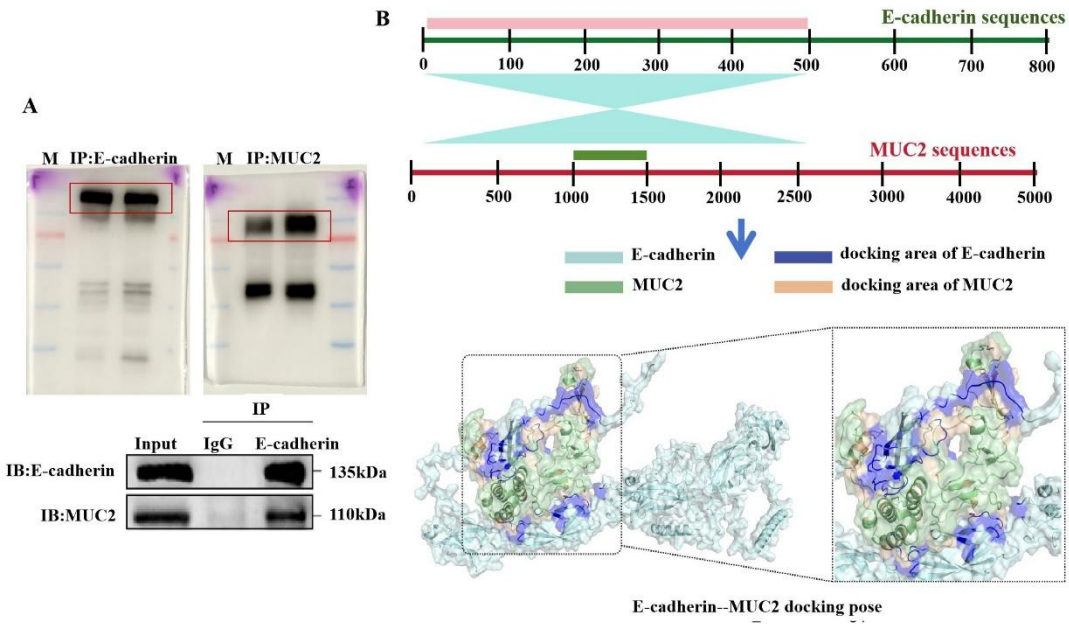
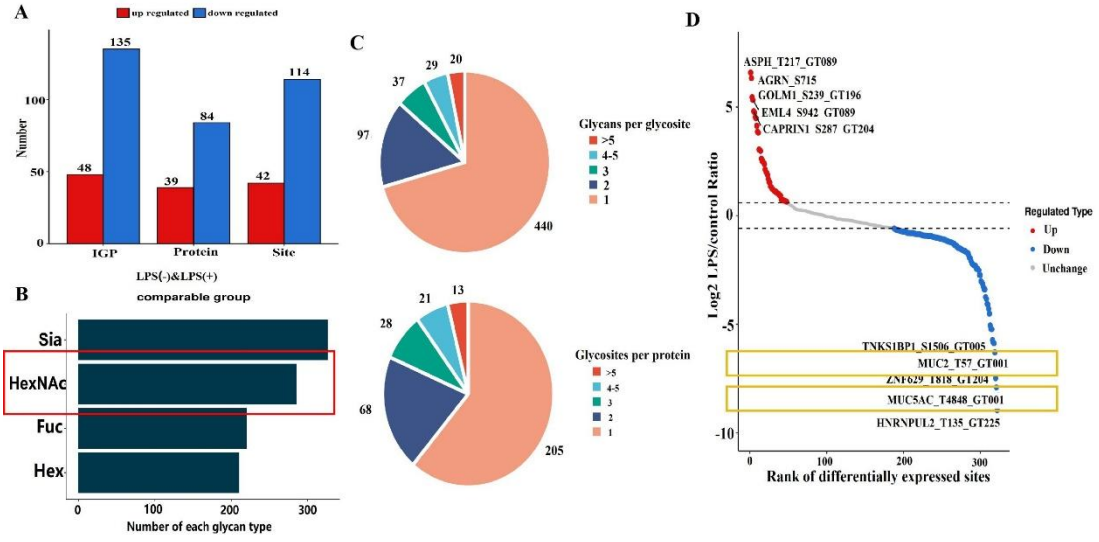


Figure 4 Analysis of O-glycopeptides of intact mucins in the LPS(-) and LPS(+) groups. A, Intact glycopeptides in the samples were obtained using MS Fragger retrieval. **B,** Based on the structure of glycan chains, they can be divided into four types: HexNAc, Hex, Fuc, and Sia. **C**, Pie chart illustrating the distribution of the number of O-glycan chains per modification site and the number of glycosylation modification sites in each protein. The figure shows the number of each O-glycan type. **D**, Ranking of differentially expressed glycosites on MUC5AC and MUC2. **E**, Changes in the MUC2 O-glycosylation chain structure after LPS treatment. Two Core-3 chains were newly added and up-regulated at 56T and 84T from MUC2 (red box). Three Core-3 chains were lost and down-regulated at 67T, 166T, and 170T from MUC2 (red box) in the LPS(+) group. Two Core-4 chains were newly added and up-regulated at 67T and 84T from MUC2 (blue box) in the LPS(+) group.



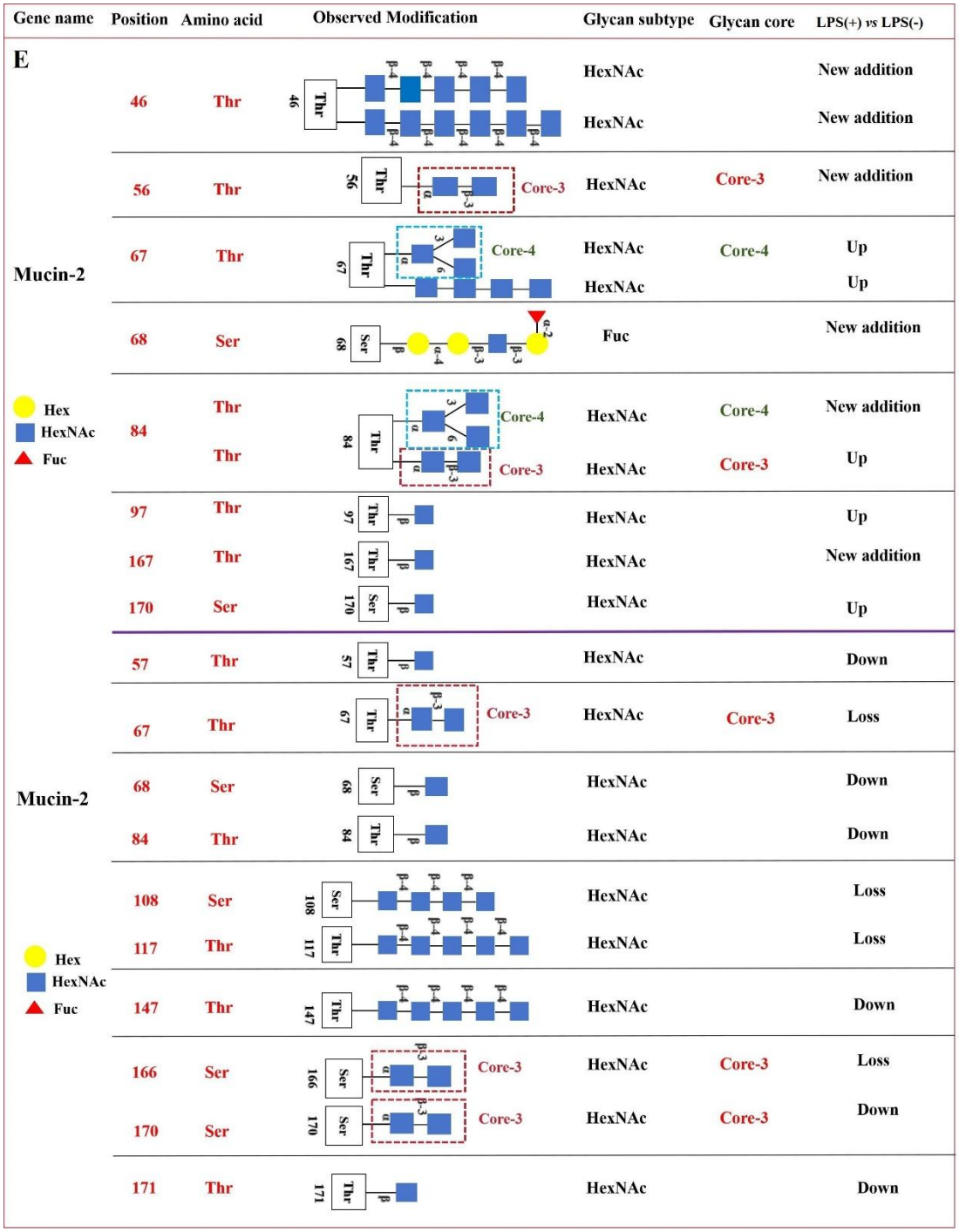


Figure 5 Expression and distribution of O-GalNAcylation and O-GlcNAcylation on MUC2 and E-cadherin in the LPS(-) and LPS(+) groups. A, C, O-GalNAcylation and O-GlcNAcylation expression on MUC2 and E-cadherin from the LPS(-) and LPS(+) group. **B,** Distribution of E-cadherin, MUC2 proteins, and O-GlcNAc, O-GalNAc observed by fluorescence microscopy in LPS(-) and LPS(+) groups (DAPI, fluorescent blue; E-cadherin, fluorescent green; MUC2, fluorescent red; O-GlcNAc/O-GalNAc, fluorescent purple).

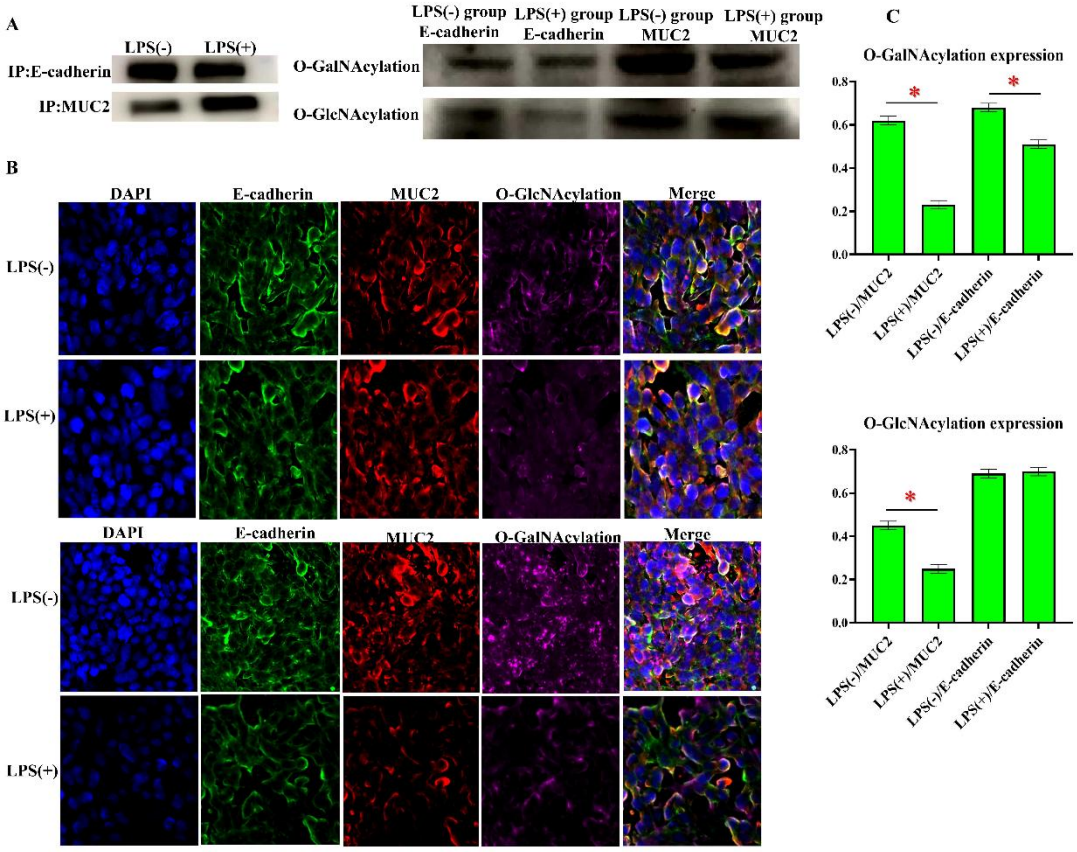
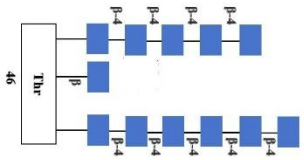
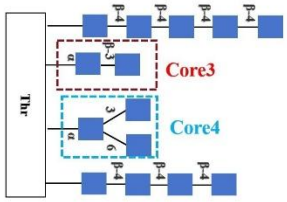
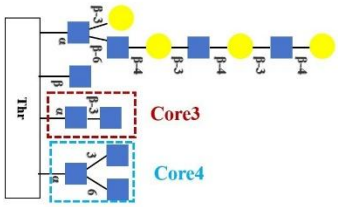
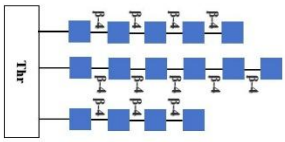
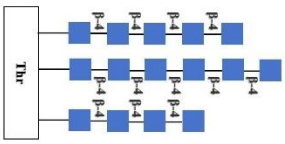
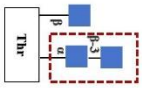
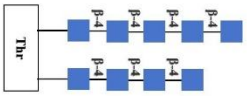
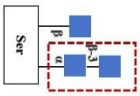


Figure 6 Analysis of the O-glycopeptides of intact mucins in the oe-GalNT3+LPS(+) and the LPS(+) groups. A, Three Core-3 chains were newly added and up-regulated at 67T, 138T, and 84T in MUC2 (red box). The Core-3 chains were down-regulated at 170T in MUC2 (red box). Two Core-4 chains were downregulated and upregulated at 67T and 84T in MUC2 (blue box) in the oe-GalNT3+LPS(+) group. **B,** Changes in the O-glycan chain of E-cadherin in the oe-GalNT3+LPS(+) group.

Gene name	Position	Amino acid	Observed Modification	Glycan subtype	Glycan core	LPS+oeGalNT3 *vs* LPS
A	35	Thr		HexNAc		Up
	46	Thr		HexNAc		Down
				HexNAc		Up
				HexNAc		Lost
Mucin-2	57	Thr		HexNAc		Up
Hex HexNAc Fuc	67	Thr		HexNAc	Core-3	New addition New addition
					Core-4	Up Down
	68	Ser		HexNAc		Up
	84	Thr		Fuc		No
				HexNAc	Core-3	Up No
					Core-4	Up
Mucin-2	102	Thr		HexNAc		New addition New addition New addition
Hex HexNAc Fuc	117	Thr		HexNAc		New addition New addition New addition
	138	Thr		HexNAc	Core-3	New addition New addition
	147	Thr		HexNAc		New addition New addition
	167	Thr		HexNAc		Down
	170	Ser		HexNAc	Core-3	Up Down
	171	Thr		HexNAc		Down

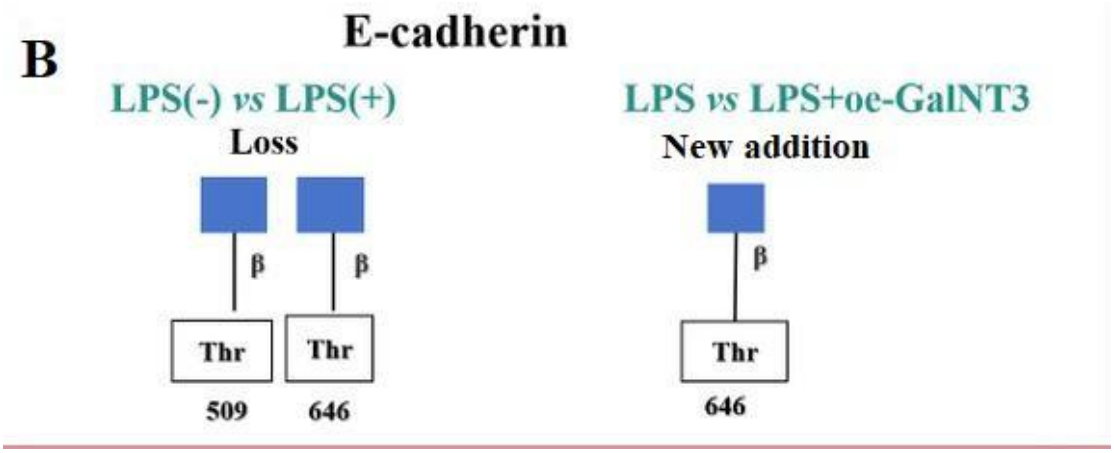
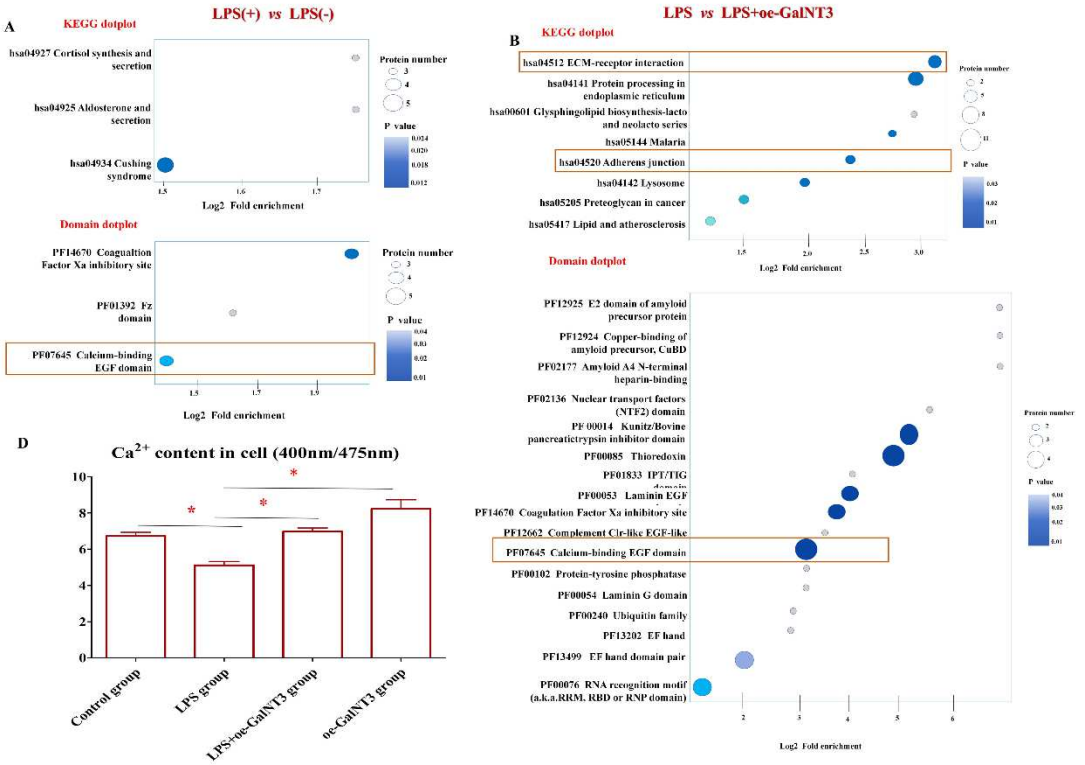


Figure 7 Functional KEGG enrichment analysis of differentially modified proteins. A, KEGG dot plot and domain dot plot in the LPS(-) *vs.* LPS(+) group. **B,** KEGG dot plot and domain dot plot in oe-GalNT3+LPS *vs.* LPS(+) group. **C**, Adherens junction signalling pathway. **D,** Ca^{2+} level of cells in the LPS(-), LPS(+), oe-GalNT3+LPS, and oe-GalNT3 groups. **E**, mRNA expression of Ca^{2+} level-regulatory factors in the LPS(-), LPS(+), oe-GalNT3+LPS, and oe-GalNT3 groups. **F,** PMCA4 (Ca^{2+}-ATPase on cell membrane) and SERCA2b (Ca^{2+}-ATPase on Rough endoplasmic reticulum membrane) protein expression in the LPS(-), LPS(+), oe-GalNT3+LPS, and oe-GalNT3 groups. **G**, The barrier function of MUC2 against LPS following overexpression of GalNT3.



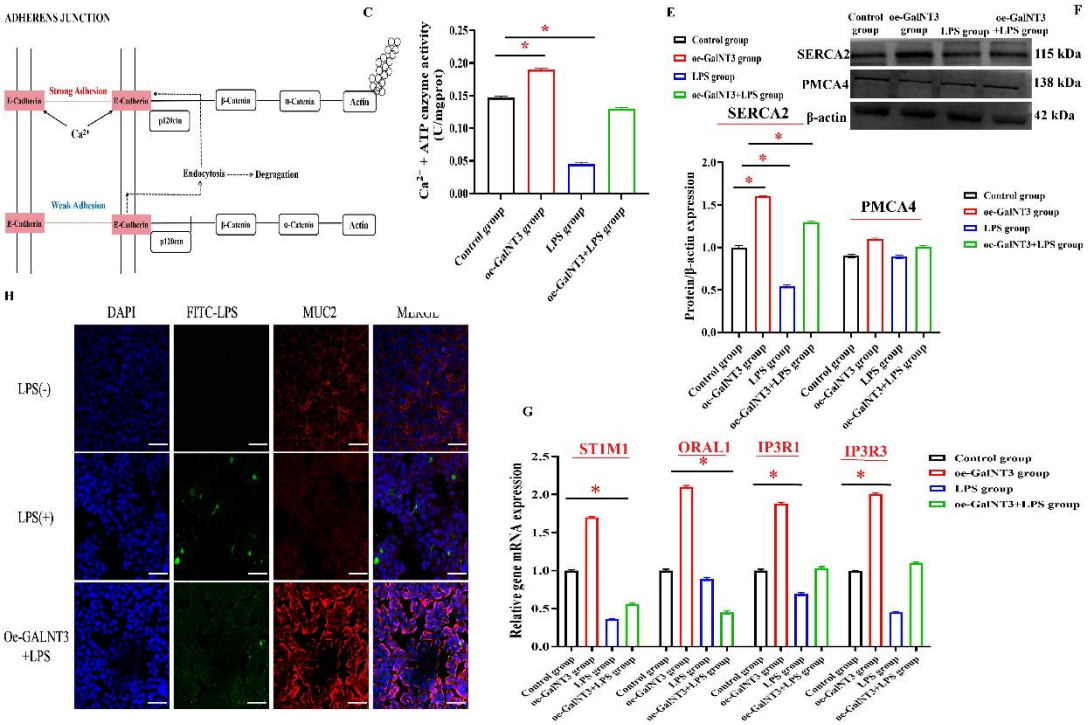


Figure 8 Expression and functional enrichment analysis of calcium-related and HexNAc genes regulated by GalNT3. A, Screening identified 14 differentially expressed genes associated with both calcium signaling pathways and HexNAc glycosylation. **B,** mRNA expression of AGRN, NUCB1, CANX, LDLR, CXCL16, CD44, PLXNB1, ERP44, CD320, ASPH, LTBP3, PRKCSH, MAN1B1, and APLP2 in the LPS(-), LPS(+), oe-GalNT3+LPS, and oe-GalNT3 groups. **C**, GO description and KEGG pathway description of AGRN, NUCB1, CANX, LDLR, CXCL16, CD44, PLXNB1, ERP44, CD320, ASPH, LTBP3, PRKCSH, MAN1B1.

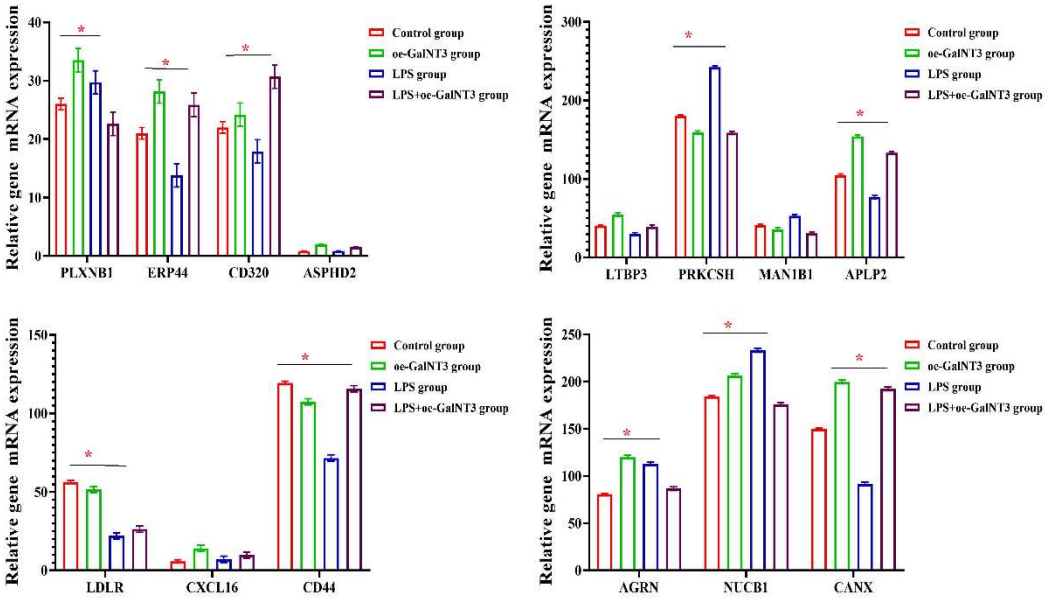
A

Calcium related

HexNAc

AGRN, NUCB1, CANX, LDLR, CXCL16, CD44, PLXNB1, ERP44, CD320, ASPH, LTBP3, PRKCSH, MAN1B1, APLP2

B

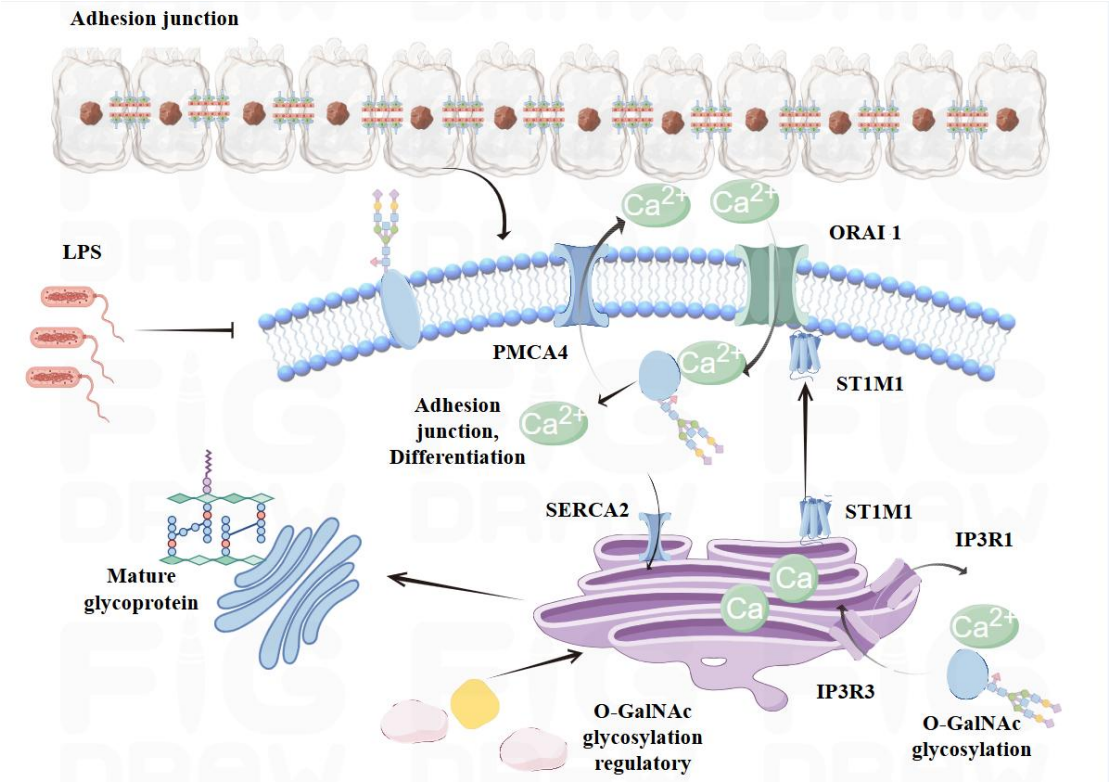


C

	GO description	KEGG pathway description
AGRN	Extracellular matrix structural constituent Structural constituent of cytoskeleton Calcium ion binding Metal ion binding	Cytoskeleton in muscle cells ECM-receptor interaction
NUCB1	Golgi apparatus Intracellular membrane-bounded organelle Extracellular region Calcium ion binding Metal ion binding	
CANX	Endoplasmic reticulum Carbohydrate binding Endoplasmic reticulum membrane Calcium ion binding Protein binding	
LDLR	Receptor-mediated endocytosis Basolateral plasma membrane Phospholipid transport Negative regulation of gene expression Positive regulation of gene expression Biosynthetic process Lipid metabolic process Negative regulation of protein metabolic process Endolysosome membrane Regulation of protein metabolic process Endosome membrane Calcium ion binding Golgi apparatus	Cushing syndrome Bile secretion Cholesterol metabolism Ovarian steroidogenesis Endocytosis Toxoplasmosis Cortisol synthesis and secretion Aldosterone synthesis and secretion Lipid and atherosclerosis
CD320	Receptor-mediated endocytosis Basolateral plasma membrane Phospholipid transport Negative regulation of gene expression Positive regulation of gene expression Biosynthetic process Lipid metabolic process Negative regulation of protein metabolic process Endolysosome membrane Regulation of protein metabolic process Endosome membrane Calcium ion binding Golgi apparatus	
LTBP3	Collagen-containing extracellular matrix Calcium ion binding Extracellular region Transforming growth factor beta binding	
MAN1B1	Carbohydrate metabolic process Acting on glycosyl bonds Calcium ion binding Metal ion binding Glycoprotein metabolic process	

	GO description	KEGG pathway description
CXCL16	Positive regulation of cell migration Receptor-mediated endocytosis Low-density lipoprotein receptor activity Extracellular region Extracellular space Plasma membrane Positive regulation of cell growth G-protein coupled receptor signaling pathway Response to cytokine	Chemokine signaling pathway Cytokine-cytokine receptor interaction
CD44	Positive regulation of heterotypic cell-cell adhesion Integral component of plasma membrane Cell-matrix adhesion Focal adhesion Cellular response to fibroblast growth factor stimulus Apical plasma membrane Extracellular matrix disassembly Cell-cell adhesion Cell surface Cell adhesion Cell projection Transmembrane signaling receptor activity Extracellular matrix organization	Shigellosis MicroRNAs in cancer ECM-receptor interaction Epstein-Barr virus infection Hematopoietic cell lineage
PLXNB1	GTPase activating protein binding Negative regulation of cell adhesion Signal transduction Intracellular signal transduction Regulation of GTPase activity Positive regulation of GTPase activity G-protein coupled receptor signaling pathway GTPase activator activity Regulation of cell shape Integral component of plasma membrane	
ERP44	Protein folding Endoplasmic reticulum-Golgi intermediate compartment Endoplasmic reticulum lumen Endoplasmic reticulum membrane Glycoprotein metabolic process Response to endoplasmic reticulum stress	
ASPHD2	Integral component of membrane Metal ion binding	
PRKCSH	Macromolecular complex binding Endoplasmic reticulum Protein binding Metal ion binding Calcium ion binding	
APLP2	Cellular protein metabolic process Transition metal ion binding Endoplasmic reticulum lumen Identical protein binding	

Figure-9 O-GalNAc glycosylation relation protein regulated Ca2+ content changes following LPS treatment.



Data Availability Statement All the raw data supporting the findings of this study are available from https://zenodo.org/uploads/17470091 (DOI:10.5281/zenodo.17470091). Details are provided within the manuscript.

Author contributions Aohang Yu and Jiayue Bai developed the concept, designed the study; Chihao Wang and Chaojie Chen wrote the paper; Lu hao and Chuang Xu performed experiments; and Chenchen Wu analyzed the data.

Funding This research was funded by National Key R&D Program of China, grant number 2023YFD1801100 and Natural Science Foundation of Xin jiang Uygur Autonomous Region (2022D01F86) and Shaanxi Natural Science Foundation (2023-YBNY-123).

Competing interests The authors declare that they have no known competing financial interests or personal relationships that could have appeared to influence the work reported in this paper.

Amon, R, Reuven, E. M, Leviatan Ben-Arye, S. & Padler-Karavani, V. Glycans in

immune recognition and response. Carbohydr. Res. 2014, 389:115-122

Bergstrom KS & Xia L Mucin-type O-glycans and their roles in intestinal homeostasis. Glycobiology. 2013, 23:1026-1037

Crocker, P. R, Paulson, J. C. & Varki, A. Siglecs and their roles in the immune system. Nat. Rev. Immunol. 2007, 7:255-66

Corfeld, A. P. Mucins: a biologically relevant glycan barrier in mucosal protection. Biochim. Biophys. Acta. 2015, 1850:236-252

De Sordi, L, Lourenco, M. & Debarbieux, L. “I will survive”: a tale of bacteriophage-bacteria coevolution in the gut. Gut Microbes. 2019, 10:92-99

Dujian Yan, Mengru Zhou, Tian Tian, Chenchen Wu.Study repair function of mucin-2 on the tight junction protein of uterine epithelial cells under bacterial endotoxins.Toxicon. 2024,252:108-121

Fatma Sanli, Arzu Tatar, Betul Gundogdu, Omer Faruk Karatas.IP3R1 dysregulation via mir-200c-3p/SSFA2 axis contributes to taxol resistance in head and neck cancer.European Journal of Pharmacology. 2024,973:176-200

Ferraretto A, Bottani M, De Luca P, Cornaghi L, Arnaboldi F, Maggioni M, Fiorilli A, Donetti E. 2018. Morphofunctional properties of a differentiated Caco-2/HT-29 co-culture as an *in vitro* model of human intestinal epithelium. *Bioscience Reports*, 38:BSR20171497

Elizabeta Madzharova, Fabio Sabino, Konstantinos Kalogeropoulos, Chiara Francavilla, Ulrich auf dem Keller.Substrate O-glycosylation actively regulates extracellular proteolysis. Protein Science. 2024, 33: e5128

Goettig P. Effects of glycosylation on the enzymatic activity and mechanisms of proteases. Int J Mol Sci. 2016, 17:1969

Goth CK, Tuhkanen HE, Khan H, Lackman JJ, Wang S, Narimatsu Y, et al. Site-specific O-glycosylation by polypeptide N-acetylgalactosaminyltransferase 2 (GalNAc-transferase T2) co-regulates β1-adrenergic receptor N-terminal cleavage. J Biol Chem. 2017, 292:4714-26

Goth CK, Vakhrushev SY, Joshi HJ, Clausen H, Schjoldager KT. Fine-tuning limited proteolysis: a major role for regulated site-specific O-glycosylation. Trends Biochem Sci. 2018, 43:269-84

Gupta R, Leon F, Rauth S, Batra SK, Ponnusamy MP. A systematic review on the implications of O-linked glycan branching and truncating enzymes on cancer progression and metastasis. Cells. 2020, 9:446

Jayaprakash, N. G. & Surolia, A. Role of glycosylation in nucleating protein folding and stability. Biochem J. 2017, 474:2333-2347

Jiaoling Wu, Kailai Fu, Chenglin Hou, Yuxin Wang, Chengyuan Ji, Feng Xue, Jianluan Ren, Jianjun Dai, Jeremy J. Barr & Fang Tang. Bacteriophage defends murine gut from Escherichia coli invasion via mucosal adherence. Nature Communications 2024, 15:4764

Joshi, H. J. et al. Glycosyltransferase genes that cause monogenic congenital disorders of glycosylation are distinct from glycosyltransferase genes associated with complex diseases. Glycobiology. 2018, 28:284-294

Katrine T. Schjoldager, Yoshiki Narimatsu, Hiren J. Joshi, Henrik Clausen. Global view of human protein glycosylation pathways and functions. Molecular Cell Biology. 2020, 21:730-750

Larsen, I. S. B. et al. Discovery of an O-mannosylation pathway selectively serving cadherins and protocadherins. Proc. Natl Acad. Sci. USA. 2017, 114:11163-11168

Laubli, H. & Borsig, L. Altered cell adhesion and glycosylation promote cancer immune suppression and metastasis. Front Immunol. 2019, 10: 2120

Liu, S, Yang, X, Liu, Y, Wang, X. & Yan, Q. sLeX/L-selectin mediates adhesion in vitro implantation model. Mol. Cell Biochem. 2011, 350:185-192

Marsico, G, Russo, L, Quondamatteo, F. & Pandit, A. Glycosylation and integrin regulation in cancer. Trends Cancer. 2018, 4:537-552

Macauley, M. S, Crocker, P. R. & Paulson, J. C. Siglec-mediated regulation of immune cell function in disease. Nat. Rev. Immunol. 2014, 14:653-666

McEver, R. P. Selectins: lectins that initiate cell adhesion under flow. Curr. Opin. Cell Biol. 2002, 14:581-586

Mengyuan He, Xiangxiang Zhou, Xin Wang. Glycosylation: mechanisms, biological functions and clinical implications. Signal Transduction and Targeted Therapy. 2024, 9:194-223

Mingming Zhang, Liyan An, Wenxiang Hu, Zhongyang Li, Yuyun Qiang, Baoyu Zhao, Tie-suo Han, Chen-chen Wu. Mechanism of endometrial MUC2 in reproductive performance in mice through PI3K/AKT signaling pathway after lipopolysaccharide treatment. Ecotoxicology and Environmental Safety. 2022, 231: 113-123

Nystrom, E. E. L. et al. An intercrypt subpopulation of goblet cells is essential for

colonic mucus barrier function. Science. 2021, 372: eabb1590.

Paone P, Cani P. D. Mucus barrier, mucins and gut microbiota: the expected slimy partners? Gut. 2020, 69:2232-2243.

Pan F, Han L, Zhang Y, Yu Y, Liu J. 2015. Optimization of Caco-2 and HT-29 co-culture in vitro cell models for permeability studies. *International Journal of Food Science and Nutrition*, 66:680-685

Pinto D, Parameswaran R. Role of truncated O-GalNAc glycans in cancer progression and metastasis in endocrine cancers. Cancers (Basel). 2023, 15:1-14

Philip A. Bidwell,Samantha L Yuen, Ji Li, Kaja Berg, Robyn T. Rebbeck, Courtney C. Aldrich, Osha Roopnarine, Razvan L. Cornea,David D. Thomas.A Large-Scale High-Throughput Screen for Modulators of SERCA Activity. Biomolecules.2022, 12, 1789-1800

Rui Ma, Chen Peng, Wenjuan Chen, Yizhen Zhang, Yangfeng Ding, Xin Wang,Yuling Shi.SERPINB7 maintains skin barrier by regulating protein O-GalNAc glycosylation.Cell Death Discovery.2026) ,12:66-70

Steentoft, C. et al. Precision mapping of the human O-GalNAc glycoproteome through SimpleCell technology. EMBO J. 2013, 32:1478-1488

Schjoldager, K. T; Narimatsu, Y; Joshi, H. J; Clausen, H. Global View of Human Protein Glycosylation Pathways and Functions. Nat. Rev. Mol. Cell Biol. 2020, 21:729-749

Schjoldager KT, Vester-Christensen MB, Goth CK, Petersen TN, Brunak S, Bennett EP, Levery SB & Clausen H A systematic study of site-specific GalNAc-type O-glycosylation modulating proprotein convertase processing. J Biol Chem. 2011, 286:40122-40132.

Schjoldager KT & Clausen H Site-specific protein O-glycosylation modulates proprotein processing-deciphering specific functions of the large polypeptide GalNAc-transferase gene family. Biochem Biophys Acta. 2012, 1820:2079-2094

Steentoft C, Vakhrushev SY, Joshi HJ, Kong Y, VesterChristensen MB, Schjoldager KTBG, et al. Precision mapping of the human O-GalNAc glycoproteome through SimpleCell technology. EMBO J. 2013, 32:1478-88

Ten Hagen KG, Bedi GS, Tetaert D, Kingsley PD, Hagen FK, Balys MM, Beres TM, Degand P & Tabak LA Cloning and characterization of a ninth member of the UDP-GalNAc: polypeptide N-acetylgalactosaminyltransferase family, ppGaNTaseT9. J Biol Chem. 2001, 276:17395-17404

Vestweber, D. & Blanks, J. E. Mechanisms that regulate the function of the selectins and their ligands. Physiol. Rev. 1999, 79:181-213

Weiyu Li, Chunyan Hou, Yaoxiang Li, Ci Wu, and Junfeng Ma. HexNAcQuest: A Tool to Distinguish O-GlcNAc and O-GalNAc.J. Am. Soc. Mass Spectrom. 2022, 33:2008-2012

Zhang M, Wang F, Xiang Z, Huang T, Zhou, WB. LncRNA XIST promotes chemoresistance of breast cancer cells to doxorubicin by sponging miR-200c-3p to upregulate ANLN. Clin. Exp. Pharmacol. Physiol. 2020,47: 1464–1472.